

Rising the of pygmy dipole resonance in nuclei with neutron excess

G. Co', V. De Donno and C. Maieron

Dipartimento di Fisica, Università del Salento and,

INFN Sezione di Lecce, Via Arnesano, I-73100 Lecce, ITALY

M. Anguiano and A. M. Lallena

Departamento de Física Atómica, Molecular y Nuclear,

Universidad de Granada, E-18071 Granada, SPAIN

(Dated: May 6, 2009)

Abstract

The electric dipole excitation of various nuclei is calculated with a Random Phase Approximation phenomenological approach. The evolution of the strength distribution in various groups of isotopes, oxygen, calcium, zirconium and tin, is studied. The neutron excess produces $E1$ strength in the low energy region. Indexes to measure the collectivity of the excitation are defined. We studied the behavior of proton and neutron transition densities to determine the isoscalar or isovector nature of the excitation. We observed that in medium-heavy nuclei the low-energy $E1$ excitation has characteristics rather different that those exhibited by the giant dipole resonance. This new type of excitation can be identified as pygmy dipole resonance.

PACS numbers:

I. INTRODUCTION

There are experimental evidences that in nuclei with neutron excess, in addition to the well known Giant Dipole Resonance (GDR), a new type of dipole resonance appears [1–3]. Since this resonance has smaller strength than that of the GDR and exhausts only a small fraction of the energy weighted sum rule, it is called Pygmy Dipole Resonance (PDR). The PDR appears at lower energy with respect to the GDR but it is not its low-energy tail, since it has an isoscalar (*IS*) character and it is dominated by neutron excitations, while the GDR has isovector (*IV*) character with almost equal contribution of proton and neutron excitations.

The existence of a new type of resonance in nuclei is an interesting subject by itself. In the present case the interest is also related to the fact that the presence of the PDR may have some relevant consequences in the stellar r-process production of exotic nuclei [4].

We have studied how the PDR emerges when neutrons become more numerous than protons. The nuclear model adopted in our calculation is the traditional discrete Random Phase Approximation (RPA). Non relativistic [5–7] and relativistic [8, 9] RPA approaches have been used in the past to investigate the PDR. Studies of PDR have been also done with more elaborated nuclear models containing pairing [10–13] and spreading widths [14–20]. Usually these calculations have been done to make detailed investigations of the PDR characteristics in a limited set of isotopes. Our goal here is to search for general trends of the PDR in various nuclei belonging to different regions of the nuclear isotope table, from oxygen to lead. For this purpose we have defined two indexes which enable us to distinguish between PDR and GDR. We tested the validity of these investigation tools on the ^{208}Pb nucleus where we found a resonance with all the features we attribute to the PDR at about 7.7 MeV, against an experimental evidence around 7.35 MeV [2]. We applied our method to isotopic chains of oxygen, calcium, zirconium and tin. We clearly identify the emergence of the PDR in the isotopes with neutron excess.

The basic features of our model are presented in Sect. II where we also make a critical discussion of its limits. We present our results in Sect. III and in Sect. IV we summarize our work and draw our conclusions.

II. THE MODEL

In our work we adopted the phenomenological RPA approach as proposed and used by the Jülich group [21–23]. The single-particle (s.p.) basis is constructed on a Woods-Saxon well whose parameters are fixed in order to reproduce at best the s.p. energies around the Fermi surface and the charge distributions. We used the parameters of the Woods-Saxon potential given in Ref. [24]. Only the parameters of the ^{90}Zr and ^{132}Sn nuclei are new, and they are presented in Table I. We used the expression of the Woods-Saxon potential given in Ref. [24]. In our RPA calculations we used experimental s.p. energies when available.

The calculations have been done in discrete s.p. basis. The s.p. Schrödinger equation with the Woods-Saxon potential has been solved by expanding the s.p. wave functions in a harmonic oscillator basis. This produces bound states even for positive s.p. energies. We consider configuration spaces by 6 major oscillator shells for oxygen, of 8 shells for calcium and 11 shells for zirconium, tin and lead nuclei. In our phenomenological model the truncation of the s.p. configuration space is taken into account in an effective manner by the choice of the parameters of the effective interaction.

Our RPA calculations have been done with a zero range force of Landau-Midgal type,

$$V_{\text{eff}}(1, 2) = \left[v_1(r_{12}) + v_1^\rho(r_{12}) \rho(r_1, r_2) + [v_2(r_{12}) + v_2^\rho(r_{12}) \rho(r_1, r_2)] \boldsymbol{\tau}(1) \cdot \boldsymbol{\tau}(2) + v_3(r_{12}) \boldsymbol{\sigma}(1) \cdot \boldsymbol{\sigma}(2) + v_4(r_{12}) \boldsymbol{\sigma}(1) \cdot \boldsymbol{\sigma}(2) \boldsymbol{\tau}(1) \cdot \boldsymbol{\tau}(2) \right] \delta(r_{12}). \quad (1)$$

In the equation above we have indicated with $\boldsymbol{\sigma}$ and $\boldsymbol{\tau}$ the usual Pauli spin and isospin operators. The zero range character of the force implies that the $v_\alpha(r_{12})$ functions of the expression above are constants. We used the values of the constants defined in Ref. [25]. The choice of the parameters was done in two steps. First, we defined the values for the density independent terms of the expression (1). These values were fixed once for all the nuclei and they describe the properties of some specific magnetic excitations in ^{16}O and ^{208}Pb . In MeV fm³ units these values are

$$v_1 = -918; v_2 = 600; v_3 = 20; v_4 = 200 , \quad (2)$$

where the sub-indexes refer to the terms in the expression (1). In the second step we chose the parameters of the density dependent terms in order to reproduce the energies of the

collective low-lying 3^- states in ^{16}O , ^{40}Ca and ^{208}Pb nuclei. This procedure selects the values of v_1^ρ . The parameters of the isospin dependent terms v_2^ρ were chosen to reproduce the peak energies of the GDR in ^{16}O , ^{40}Ca , ^{132}Sn and ^{208}Pb . For each doubly closed shell nucleus considered, we give in Table II the values of the parameters of the density dependent terms of the force. Note that for the ^{90}Zr nucleus we used the set of values selected for ^{40}Ca .

The structure of the interaction (1) is simple if compared with the complexity of modern microscopic nucleon-nucleon interactions, as for example the Argonne V18 [26]. We tested the reliability of our results by doing calculations also with more elaborated effective nucleon-nucleon interactions. We used the finite range interactions of Refs. [25, 27] containing also tensor terms. In the excitation of the 1^- states, the differences between the results obtained with the various interactions are rather small and not relevant for the purposes of the present work. For this reason we present here only the results obtained with the interaction (1).

For a given multipolarity J^π , our RPA calculations produce a number of solutions equal to the number of particle-hole excitations, N_{ph} , compatible with the angular momentum and parity conservation rules within the given configuration space. For a single solution, of excitation energy ω , the RPA provides the set of amplitudes $X_{ph}(\omega)$ and $Y_{ph}(\omega)$ which describe the wave function of the excited state in terms of particle-hole (p-h) and hole-particle (h-p) excitations, respectively. The proper normalization of the many-body wave function implies that, for a given excited state, the RPA amplitudes are normalized as:

$$\sum_{ph=1}^{N_{ph}} [X_{ph}^2(\omega) - Y_{ph}^2(\omega)] = 1 . \quad (3)$$

In our search for states which can be identified as PDR, we singled out a few quantities which summarize the main characteristics of each state. First, for a given excited state, we calculated the relative contribution of protons and neutrons to the normalization (3). These contributions, indicated as $N(\pi)$ and $N(\nu)$ in the following, are obtained from Eq. (3) by summing over p-h pairs for protons, or, respectively, neutrons only.

Second, we defined an index to measure the degree of collectivity of a specific excited state. In the ideal collective state all the p-h excitation pairs contribute with the same statistical weight. In this case, all the $X_{ph}^2(\omega) - Y_{ph}^2(\omega)$ terms of Eq. (3) would contribute $1/N_{ph}$. From these considerations we defined a collectivity index as

$$\mathcal{D} = N^*/N_{ph} , \quad (4)$$

where N^* is the number of states with $(X_{ph}^2(\omega) - Y_{ph}^2(\omega)) \geq 1/N_{ph}$. The two extreme values of \mathcal{D} are 1 in the fully collective case, and $1/N_{ph}$ when the excitation is produced by a single p-h pair.

The definition of \mathcal{D} , Eq. (4), depends on the number of p-h excitations N_{ph} , and this latter quantity is related to the size of the configuration space. The values of the index \mathcal{D} must be used to compare excited states calculated within the same configuration space. To gauge the values of \mathcal{D} indicating a high degree of collectivity, we calculated \mathcal{D} for the collective low-lying 3^- states of various doubly closed shell nuclei. These values are given in Table III and are our reference values.

The collectivity of a state is not only related to the value of the X and Y amplitudes, but also to the coherence of the p-h pairs in constructing transition amplitudes. For this reason we also calculated the transition densities

$$\rho(EJ; \omega, r) = \sum_{ph} [X_{ph}(\omega) + Y_{ph}(\omega)] \rho_{ph}^J(r) , \quad (5)$$

with

$$\rho_{ph}^J(r) = (-1)^{j_p + \frac{1}{2}} \frac{\widehat{j}_p \widehat{J} \widehat{j}_h}{\sqrt{4\pi}} \begin{pmatrix} j_p & J & j_h \\ \frac{1}{2} & 0 & -\frac{1}{2} \end{pmatrix} R_p(r) R_h(r) . \quad (6)$$

In the equation above we have indicated with $R(r)$ the radial part of the s.p. wave functions, with j their angular momenta, we used the symbol $\widehat{j} = \sqrt{2j+1}$ and the traditional symbol to indicate the Wigner 3-j coefficient.

We calculated separately the proton and neutron transition densities by limiting the sum of Eq. (5) to proton or neutron pairs only. The transitions densities for the low-lying 3^- states of the various doubly closed shell nuclei are shown in Fig. 1. The full lines indicate the proton densities, while the dashed lines the neutron densities. The structure of the various densities becomes more complicated the heavier is the nucleus. Despite these differences, in all the cases shown in the figure the *in phase* behavior of the two types of density is evident. This indicates the *IS* character of the transition. The *IS* structure of these states is confirmed by the fact that the energies eigenvalues are sensitive only to scalar terms of the interaction, v_1 and v_1^ρ of Eq. (1).

Finally, we characterize each state by its $B(E1)$ value and by the ratio \mathcal{R} between the $B(E1)$ value of the specific state and the total $B(E1)$ strength. We prefer to consider this ratio, rather than making a comparison with the Thomas-Reiche-Kuhn energy weighted

sum rule, because our approach is not self-consistent, and in addition it uses a truncated s.p. configuration space. In any case, our results satisfy the sum rule at the 5% level.

In our work, we used the following strategy. The set of s.p. wave functions, and the parameters of the effective nucleon-nucleon interaction, were chosen to reproduce some properties of the ^{16}O , ^{40}Ca , ^{90}Zr , ^{132}Sn and ^{208}Pb doubly magic nuclei, as we have discussed above. Around each doubly magic nucleus we constructed a set of isotopes by increasing or decreasing, within the chosen configuration space, the number of neutron levels forming the ground state. Since we work with a spherical basis, the difference between the number of neutrons of each isotope is $2j + 1$, where j is the angular momentum of the level with higher energy. We considered only isotopes which have been experimentally identified. For each isotopic chain we used the effective interaction and s.p. basis adjusted to reproduce the properties of the doubly magic nucleus of the chain. The number of neutrons was changed by considering a different number of fully occupied s.p. levels.

Before presenting the results of our calculations we want to critically discuss the basic features and the limits of our model. The first point is related to the choice of a discrete, and restricted, configuration space. We have recently verified the large sensitivity of the RPA results to the truncation of the configuration space [25, 27]. Only a proper treatment of the continuum can provide numerically stable RPA results. This is a big problem in self-consistent calculations where the effective nucleon-nucleon interaction used in the RPA is the same one also used to build the s.p. basis by means of a Hartree-Fock calculation. In our phenomenological approach we use s.p. bases constructed on a Woods-Saxon potential, and effective interactions chosen to reproduce the energies of some specific excited states. The effects of the truncation of the configuration space are effectively taken into account by the choice of the parameters of the interaction. Therefore our effective interactions are strictly related to the configuration space. In our calculations all the nuclei of a given isotopic chain are described by using the same parameterization of the nucleon-nucleon interaction and the same set of s.p. wave functions. This ensures numerical stability at the price of a rigid use of the s.p. wavefunctions. A Hartree-Fock approach would be more flexible. In any case, we studied the ground states of the oxygen isotopes ^{16}O , ^{22}O , ^{24}O , ^{28}O by using a spherical Hartree-Fock approach [25, 28] with the Gogny D1 interaction [29], and we did not find relevant differences in the occupied s.p. wave functions of the ^{16}O core.

The second point we would like to discuss is related to the fact that our calculations

do not consider effects beyond one-particle one-hole (1p-1h) excitations, even though in the literature there are now quite a few calculations of the PDR excitations where these effects are taken into account [1–3, 15–18]. The inclusion of p-h excitations beyond those considered by the RPA produces two effects related to the real and imaginary part of the self-energy. The real part of the self-energy changes the position of the resonance. In our approach this effect is taken into account by using phenomenological s.p. energies and effective interactions. The imaginary part generates a spreading of the width of the resonances obtained in RPA. Our approach cannot simulate this effect.

Finally, we consider pairing and deformation. Our phenomenological approach cannot simulate these effects. For this reason, besides doubly magic nuclei, we have studied only those nuclei with fully occupied s.p. levels. In this case, we expect that the spherical symmetry of the nucleus is almost restored, and also pairing effects should be smaller than in nuclei with the partially occupied levels.

An accurate description of the experimental data requires the inclusion of terms which consider the spreading of the resonance width. However, despite of its simplicity, our model should predict the position of the resonance, its total strength, the degree of collectivity and the relative importance of proton and neutron excitations. These are the quantities we have considered in our work and they are presented and discussed in the next section.

III. SPECIFIC APPLICATIONS

In this section we present the results obtained by applying our model to a set of isotopic chains built around the doubly magic nuclei ^{16}O , ^{40}Ca , ^{90}Zr and ^{132}Sn . Before doing that, we discuss the ^{208}Pb results. In this nucleus we identify the PDR, therefore the values of the collectivity indexes, and the behavior of the proton and neutron transition densities, can be used as references for the results obtained for the other nuclei.

In panel (a) of Fig. 2 we present the $B(E1)$ values of the ^{208}Pb nucleus as a function of the excitation energy ω . The figure shows the GDR region which has its maximum at 14.67 MeV and a set of peaks at lower energy which we identify with the PDR region. We discuss with some detail the characteristics of the states which are indicated by the arrows in panel (a). The energy value of the first state is 6.58 MeV. For this state we found $\mathcal{D}=0.049$ and $N^*=10$. The proton contribution to the normalization of the wavefunction is $N(\pi)=0.026$,

therefore the neutron contribution is $N(\nu) = 0.974$. The proton and neutron transition densities for this state are shown in panel (b) of the figure. The characteristics of the other state are $\omega = 7.77$ MeV, $\mathcal{D} = 0.049$, $N^* = 10$, $N(\pi) = 0.238$ and $N(\nu) = 0.762$, and its transition densities are shown in panel (c) of the figure. For both states, the proton and neutron transition densities are *in phase*, which is the typical behavior of the *IS* excitation. The behavior of these transition densities, are rather different from those of the states forming the GDR. As typical example, we discuss here only the state at 14.67 MeV. For this state we obtain $\mathcal{D} = 0.073$, and $N^* = 15$, two values indicating a slightly higher collectivity with respect to that of the PDR. The contributions to the normalization of the wave functions are $N(\pi) = 0.682$ and $N(\nu) = 0.318$. The transition densities for the GDR state are shown in panel (d) and they have an *out of phase* behavior indicating the *IV* nature of the excitation.

Photon scattering experiments on ^{208}Pb have identified, in addition to the well known GDR peaked at 13.5 MeV [30], a small dipole resonance around 7.35 MeV which has been interpreted as PDR [2]. In our calculations we found a large resonance above 13.5 MeV which contributes for about the 70% of the total dipole strength, and a tiny resonance with centroid energy at about 7.2 MeV which carries about the 5% of the total strength. The two resonances have a similar degree of collectivity, though the resonance at smaller energy shows an *IS* structure while the other resonance has an *IV* structure. In the PDR, the contribution of neutron p-h pairs is slightly larger than that of the protons, while in the GDR the neutron and proton contributions are more equilibrated.

In the following study, we use the values of the indexes \mathcal{D} , $N(\pi)$ and $N(\nu)$ presented above as a guide to identify the presence of a collective excitation, and we identify the *IS* or *IV* character of the excitation by analyzing the behavior of the proton and neutron transition densities.

We start our discussion by considering the ^{22}O , ^{24}O , ^{28}O nuclei, obtained from the ^{16}O core by filling the neutron $1d_{5/2}$, $2s_{1/2}$ and $1d_{3/2}$ s.p. levels respectively. The $B(E1)$ distributions for these isotopes are presented in Fig. 3. The isotopes with neutron excess show a rich structure at excitation energies below the GDR peak. The values of the collectivity indexes of the states indicated by the arrows in the figure are given in Table IV. In this table we also give the ratio \mathcal{R} between the $B(E1)$ of the indicated state and the global $B(E1)$ strength.

The values presented in Table IV give some indication of collectivity of the states below the GDR. In the three heavier isotopes of the ^{16}O , the states around 11, 12 MeV have a

relatively large degree of collectivity. For this reason we analyzed their transition densities, and we found that they have an *IV* structure, as it is shown in Fig. 4. For these three nuclei we compare the transition densities of the GDR peak with that of the state with the largest $B(E1)$ value. The *out of phase* behavior of the densities indicates that these states are produced by the fragmentation of the GDR and they are not a new type of excitation.

The situation is rather different for the other isotopic chains we have studied. The results for the calcium chain are presented in Figs. 5 and 6 and in Table V. In our study, we considered the ^{48}Ca and ^{52}Ca isotopes obtained from the ^{40}Ca core by filling the neutron $1f_{7/2}$ and $2p_{3/2}$ s.p. levels. The $B(E1)$ distributions of these three isotopes are shown in Fig. 5. As we have already observed for the oxygen case, also in this case the presence of excess neutrons produces $E1$ strength at energies lower than those of the GDR. We have repeated the study of these states in analogy to what we have done for lead and oxygen, and the values of the collectivity indexes for the states indicated by the arrows are given in Table V. The states at the peak of the GDR show a degree of collectivity comparable with that of the 3^- state (see Table III). Proton and neutron p-h pairs contribute to the excitation with almost equal weight. The structure of the lower energy states is different. There is a certain degree of collectivity, but it is smaller than that of the states just described. In addition it is evident that these states are dominated by neutron excitations. The different structure of these two type of states is emphasized by the transition densities, which are shown in Fig. 6. The low energy states show an *in phase* behavior, typical of the IS transition, while the higher energy states have the typical *IV out of phase* behavior. All these remarks indicate that the low energy states are not produced by the fragmentation of the GDR, as it happens for the oxygen isotopes, but they are a new type of excitation.

When the nucleon number increases, the features related to the rising of the PDR become more evident. We found an excellent example of this fact in the Zr chain. In Fig. 7 we show the $B(E1)$ distributions for the ^{90}Zr , ^{98}Zr , ^{104}Zr , ^{108}Zr , and ^{110}Zr isotopes. We constructed this isotopic chain starting from the ^{90}Zr core and filling the neutron $1g_{7/2}$, $2d_{5/2}$, $2d_{3/2}$ and $3s_{1/2}$ s.p. levels respectively. In these calculations we used the same interaction adopted for the Ca calculations.

With the increasing of the number of neutrons, we observe a fragmentation of the $B(E1)$ distributions. There is a fragmentation of the GDR and a rising of new strength at low energy. In ^{90}Zr the most important state is at 17.89 MeV, and is indicated by the arrow in

Fig. 7. This state carries about the 30% of the total $B(E1)$ strength. In the ^{110}Zr nucleus, this state is not any more the most important one, and it is responsible only for about the 9% of the total strength. The remaining part of the GDR strength has been redistributed between states with slightly smaller energies.

In our discussion we consider three specific states for each isotope, and we indicated them in Fig. 7 by the arrows. The values of the collectivity indexes for these states are presented in Table VI. We have followed the evolution of these states in all the isotopic chain. The lower energy states have extremely small $B(E1)$ values in the ^{90}Zr and ^{98}Zr isotopes, as it is shown by the values of \mathcal{R} . Their contributions to the total strength increase with increasing the neutron number. Both states are neutron dominated. On the contrary, the most important state of the GDR in ^{90}Zr has an almost equal contribution of proton and neutron components. The proton contribution becomes smaller with the increase of the neutron number, but still it remains remarkable. The low-lying states have an *IS* behavior, while the states of the giant resonance have an *IV* behavior. As an example of the results we have obtained, we show in Fig. 8 the transition densities for the 8.3 - 8.4 MeV states, and those of the peak in ^{90}Zr at 17.89 MeV. The proton and neutron transition densities of the lower energy states clearly show an *IS in phase* behavior, contrary to the *out of phase* behavior of the 17.89 MeV state in ^{90}Zr indicating the *IV* character of the GDR.

As a last application of our model we show the results regarding a Sn isotopic chain. These calculations are of interest since the PDR has been recently identified around 10 MeV in tin isotopes [1]. In the case of the Sn chain, the doubly magic nucleus is the heaviest of the chain, the ^{132}Sn , which, obviously has the largest number neutrons. We obtain the other isotopes by removing neutrons from the $2d_{3/2}$, $1h_{11/2}$, $3s_{1/2}$ and $2d_{5/2}$ levels, to obtain the ^{128}Sn , ^{116}Sn , ^{114}Sn and ^{108}Sn nuclei, respectively.

The $B(E1)$ distributions for these isotopes are shown in Fig. 9. For all the nuclei, we found, in addition to the GDR, also a group of states which appear at lower energies. We give in Table VII the values of the various indexes for some characteristic states. The states at about 7.8 MeV and 8.4 MeV have large $B(E1)$ values also in the lighter isotopes. We found it interesting to follow the development of the state at about 10 MeV. This state has negligible $B(E1)$ values in all the isotopes up to ^{116}Sn . Its $B(E1)$ value becomes visible in ^{128}Sn , about the 0.2 % of the global $B(E1)$ contribution, and it further increases in ^{132}Sn . With respect to the other tin isotopes, the additional neutrons of ^{132}Sn produce a relevant

contribution for this state, as indicated by the relatively large value of N^* shown in Table VII. We show in Fig. 10 the transition densities for these 10 MeV states in the various isotopes, and for the sake of comparison, also that of the state at the peak of the GDR in ^{132}Sn . The relative behavior of the proton and neutron transition densities clearly shows the *IS* structure of the states below the GDR and the *IV* structure of the 16.92 state in ^{132}Sn .

The results presented above indicate that in medium heavy nuclei with neutron excess, a new type of dipole resonance appears, with the characteristics we attribute to the PDR, and that the presence of this resonance becomes more important with the increase of the neutron number. We further investigated this point by considering the ratio \mathcal{R}_{int} between the integrated $B(E1)$ low energy strength and the total strength. We calculated the numerator of \mathcal{R}_{int} by summing all the $B(E1)$ values located below the values indicated by the dashed lines in Figs. 5, 7 and 9, and the total strength in the denominator by summing over the whole energy range shown in the figures.

In Fig. 11 \mathcal{R}_{int} is plotted against the number of neutrons in excess with respect to the doubly magic core of the Ca, Zr and Sn isotopic chains. These results clearly show an increase of the relative $E1$ strength in the low energy region with increasing neutron number.

The number of Ca isotopes we have considered is too small to allow a systematic study of the dependence of \mathcal{R}_{int} on the neutron excess, whereas for the Zr chain we observe a monotonic growth. The behavior of the Sn isotopic chain is more complicated. A linear growth is observed for $A=108-116$, then the value of \mathcal{R}_{int} for ^{128}Sn is almost equal to that for ^{116}Sn , and it starts to grow again, but more slowly, when passing from ^{128}Sn to ^{132}Sn . This behavior resembles that observed in Ref. [9] (see also [31]), where, within a relativistic RPA framework, a linear correlation between the ratio of the low-energy to high-energy dipole strength and the neutron skin of the Sn isotopes was obtained for $A \leq 120$, followed by an apparent mild anticorrelation for $120 \leq A \leq 132$. The latter was attributed to the filling of the $1h_{11/2}$ neutron orbital.

In the upper panel of Fig. 12 we show again the ratio \mathcal{R}_{int} for various Sn isotopes, but now as a function of the neutron skin calculated as a difference between the neutron and proton root mean square radii, $R_n - R_p$. The nuclei considered have, from left to right, $A = 108, 114, 116, 128$ and 132 . In the lower panel of the figure, we relate these neutron skins to the isotope mass number. Although we only consider isotopes with fully occupied s.p. levels, our results confirm the findings of Ref. [9], except for the heaviest isotopes. In

fact, we do not find any anticorrelation effect since \mathcal{R}_{int} mildly increases in going from ^{128}Sn to ^{132}Sn .

IV. DISCUSSION AND CONCLUSIONS

We have studied the electric dipole excitation spectra of several isotopes of oxygen, zirconium and tin nuclei, searching for a possible appearance of the PDR. The calculations were done for isotopes with fully occupied s.p. levels using a traditional phenomenological RPA approach without pairing effects. In Sect. II, we have critically discussed merits and faults of our approach which we think to be reliable in predicting position and total strength of the resonance.

The dipole excited states have been studied by analyzing their collectivity, their isospin character and the relevance on neutron and proton p-h excitations. We have defined an index \mathcal{D} , see Eq. (4), which quantifies the degree of collectivity. From the study of the proton and neutron transition densities, Eq. (5), we have identified the *IS* character with the *in phase* behavior of the two transition densities, while the *out of phase* behavior indicates the *IV* character. We should mention here that we have also investigated the vorticity of the excitations [32], as it has been suggested in [2], but we did not find significant differences between the results in the PDR and GDR regions. Our work consisted in studying 1^- excitations in isotopic chains built around doubly closed shell nuclei, to identify the possible presence of PDR. The signals we searched for identifying the PDR are high degree of collectivity, *IS* character and neutron dominated excitation.

We have first applied our model to oxygen isotopes where we observed an increase of the *E1* strength at low energies. These states did not satisfy our identification criteria. We observed a fragmentation of the GDR, rather than the rising of a new type of excitation mode. This result disagrees with the findings of Ref. [5], where the calculations were done in a fully self-consistent Hartree-Fock plus RPA approach with Skyrme-like interactions. The problem is still open. In any case, we should point out that the oxygen nuclei are relatively light and in our approach the number of p-h pairs responsible for the low-lying excitations is so small that it is difficult to consider these excited states as collective excitation of the nucleus (see the values of N^* in Table IV).

We found positive results for all the other isotopic chains we have investigated. Our cal-

culation for the ^{48}Ca produces strength around 8.5 MeV in agreement with the experimental findings of Ref. [3] and with the results of Ref. [6]. Also the results in tin isotopes show low energy strength and confirm the experimental finding of Ref. [1]. We identify this excitation as PDR as it has been done in [8]. This result is in contrast with the findings of Ref. [15], obtained with self-consistent calculations which consider also effects beyond the RPA, in terms of phonon coupling. The authors of Ref. [15] indicate that few p-h excitations are responsible for the low energy states, while our calculations give quite a relevant collectivity for these states.

In the study of the zirconium isotopes we have found a handbook example of the role played by the neutrons in excess. The contribution of the state at about 8.5 MeV to the $B(E1)$ strength becomes relevant only in the heavier isotopes, where the neutrons in excess strongly contribute to the excitation and make it collective.

Our calculations clearly indicate that the appearance of the PDR is a common feature of medium- heavy-nuclei. By studying the ratio between the low energy and the total integrated $B(E1)$ strength we have seen that the relevance of the PDR increases with increasing neutron number.

Acknowledgments

We thank D. Gambacurta and J. Speth for useful discussions. This work has been partially supported by the Spanish Ministerio de Ciencia e Innovación under contract FPA2008-04688 and by the Junta de Andalucía (FQM0220).

[1] P. Adrich, et. al., *Phys. Rev. Lett.* 95 (2005) 132501.

[2] N. Ryezayeva, et. al., *Phys. Rev. Lett.* 89 (2002) 272502.

[3] T. Hartmann, et. al., *Phys. Rev. Lett.* 93 (2004) 192501.

[4] S. Goriely, *Phys. Lett. B* 436 (1998) 10.

[5] F. Catara, E. G. Lanza, M. A. Nagarajan, A. Vitturi, *Nucl. Phys. A* 624 (1997) 449.

[6] J. Chambers, E. Zaremba, J. P. Adams, B. Castel, *Phys. Rev. C* 50 (1994) R2671.

[7] A. M. Oros, K. Heyde, C. DeCoster, B. Decroix, *Phys. Rev. C* 57 (1998) 990.

[8] D. Vretenar, N. Paar, P. Ring, G. A. Lalazissis, *Nucl. Phys. A* 692 (2001) 496.

[9] J. Piekarewicz, *Phys. Rev. C* 73 (2006) 044325.

[10] S. Kamerdzhev, R. J. Liotta, E. Litvinova, V. Tselyaev, *Phys. Rev. C* 58 (1998) 172.

[11] S. Goriely, E. Khan, *Nucl. Phys. A* 706 (2002) 217.

[12] G. Giambrone, S. Scheit, F. Barranco, P. Bortignon, G. Colò, D. Sarchi, E. Vigezzi, *Nucl. Phys. A* 726 (2005) 3.

[13] S. Goriely, E. Khan, M. Samyn, *Nucl. Phys. A* 739 (2004) 331.

[14] G. Colò, P. F. Bortignon, *Nucl. Phys. A* 696 (2001) 427.

[15] D. Sarchi, P. F. Bortignon, G. Colò, *Phys. Lett. B* 601 (2004) 27.

[16] N. Tsoneva, H. Lenske, C. Stoyanov, *Nucl. Phys. A* 731 (2004) 273.

[17] N. Tsoneva, H. Lenske, C. Stoyanov, *Phys. Lett. B* 586 (2004) 213.

[18] N. Tsoneva, H. Lenske, *Prog. Part. Nucl. Phys.* 59 (2006) 317.

[19] E. Litvinova, P. Ring, D. Vretenar, *Phys. Lett. B* 647 (2007) 111.

[20] V. Tselyaev, J. Speth, F. Grümmer, S. Krewald, A. Avdeenkov, E. Litvinova, G. Tertychny, *Phys. Rev. C* 75 (2007) 014315.

[21] J. Speth, E. Werner, W. Wild, *Phys. Rep.* 33 (1977) 127.

[22] G. A. Rinker, J. Speth, *Nucl. Phys. A* 306 (1978) 360.

[23] J. Speth, V. Klemt, J. Wambach, G. E. Brown, *Nucl. Phys. A* 343 (1980) 382.

[24] F. Arias de Saavedra, C. Bisconti, G. Co', A. Fabrocini, *Phys. Rep.* 450 (2007) 1.

[25] V. De Donno, G. Co', C. Maier, M. Anguiano, A. M. Lallena, M. Moreno-Torres, *Phys. Rev. C* 79 (2009) 044311.

[26] R. B. Wiringa, V. G. J. Stoks, R. Schiavilla, *Phys. Rev. C* 51 (1995) 38.

- [27] V. De Donno, Nuclear excited states within the random phase approximation theory, Ph.D. thesis, Università del Salento (Italy), unpublished (2008).
- [28] A. R. Bautista, G. Co', A. M. Lallena, Nuov. Cim. A 112 (1999) 1117.
- [29] J. Dechargè, D. Gogny, Phys. Rev. C 21 (1980) 1568.
- [30] J. Ahrens, et al., Nucl. Phys. A 251 (1975) 479.
- [31] N. Paar, D. Vretenar, E. Khan, G. Colò, Rept. Prog. Phys. 70 (2007) 691–794.
- [32] D. G. Ravenhall, J. Wambach, Nucl. Phys. A 475 (1987) 468.

	V_0	R_0	a_0	V_{LS}	R_{LS}	a_{LS}	R_c
^{90}Zr	π	55.88	5.69	0.73	7.70	5.68	0.73
	ν	48.12	5.69	0.73	7.70	5.68	0.73
^{132}Sn	π	58.85	6.40	0.70	8.95	6.40	0.70
	ν	47.50	6.10	0.70	5.50	6.10	0.70

Table I: Parameters of the Woods-Saxon potential for the ^{90}Zr and ^{132}Sn nuclei. The values of V_0 and V_{LS} are expressed in MeV, all the others in fm. As in the traditional nuclear structure convention, we indicate with π and ν the proton and neutron parameters, respectively. The explicit expression of the Woods-Saxon potential is given in Ref. [24].

^{16}O	^{40}Ca	^{90}Zr	^{132}Sn	^{208}Pb
v_1^ρ	436.4	492.3	492.3	585.0
v_2^ρ	-310.0	-150.0	-150.0	-50.0
				0.0

Table II: Values of the parameters of the density dependent terms of the interaction Eq. (1), in MeV fm³.

	^{16}O	^{40}Ca	^{132}Sn	^{208}Pb	
ω	6.12	3.74	4.34	2.63	
N^*	5	10	27	40	
\mathcal{D}	0.192	0.135	0.095	0.119	
$N(\pi)$	0.501	0.568	0.187	0.362	
$N(\nu)$	0.499	0.432	0.813	0.638	

Table III: Values of the collectivity indexes for the low-lying 3^- states of the doubly closed shell nuclei we considered. The values of the excitation energies ω are expressed in MeV, \mathcal{D} is defined in Eq. (4) and N^* is the numerator of that equation. With $N(\pi)$ and $N(\nu)$ we have indicated respectively the proton and neutron contribution to the normalization (3), clearly $N(\pi) + N(\nu) = 1$.

	ω [MeV]	N^*	\mathcal{D}	$N(\pi)$	$N(\nu)$	\mathcal{R}
^{16}O						
	23.70	4	0.143	0.480	0.520	0.855
^{22}O						
	7.46	1	0.003	0.006	0.074	0.017
	11.68	5	0.152	0.074	0.926	0.106
	22.17	5	0.152	0.459	0.541	0.229
^{24}O						
	6.36	2	0.057	0.020	0.980	0.095
	12.01	6	0.171	0.546	0.454	0.018
	20.40	9	0.257	0.530	0.490	0.273
^{28}O						
	6.29	3	0.077	0.035	0.965	0.079
	11.28	8	0.205	0.162	0.838	0.096
	20.36	10	0.256	0.634	0.366	0.348

Table IV: Values of the collectivity indexes for the 1^- states of the various oxygen isotopes identified by the arrows in Fig. 3. The meaning of the various indexes is the same as in Table III. We also show the ratio \mathcal{R} between the $B(E1)$ of the specific state and the total $B(E1)$ strength.

ω [MeV]	N^*	\mathcal{D}	$N(\pi)$	$N(\nu)$	\mathcal{R}
^{40}Ca					
20.69	8	0.133	0.670	0.340	0.409
^{48}Ca					
8.73	5	0.077	0.096	0.904	0.006
18.62	11	0.170	0.521	0.479	0.684
^{52}Ca					
8.65	3	0.045	0.020	0.980	0.063
18.21	9	0.134	0.503	0.497	0.664

Table V: Same as in Table IV for the 1^- states of the various calcium isotopes identified by the arrows in Fig. 5.

ω [MeV]	N^*	\mathcal{D}	$N(\pi)$	$N(\nu)$	\mathcal{R}
^{90}Zr					
7.41	4	0.026	0.022	0.978	0.000
8.42	7	0.045	0.024	0.976	0.000
17.89	19	0.123	0.656	0.344	0.316
^{98}Zr					
7.53	8	0.050	0.013	0.987	0.005
8.45	7	0.043	0.019	0.981	0.000
17.89	18	0.111	0.678	0.322	0.313
^{104}Zr					
7.52	6	0.036	0.011	0.989	0.004
8.45	11	0.066	0.025	0.975	0.016
17.79	13	0.078	0.818	0.182	0.133
^{108}Zr					
7.57	6	0.035	0.011	0.989	0.005
8.35	11	0.065	0.025	0.975	0.017
17.58	10	0.059	0.251	0.749	0.093
^{110}Zr					
7.45	7	0.041	0.004	0.996	0.012
8.29	13	0.076	0.020	0.980	0.016
17.58	10	0.058	0.250	0.750	0.092

Table VI: Same as in Table IV for the 1^- states of the various zirconium isotopes identified by the arrows in Fig. 7.

ω [MeV]	N^*	\mathcal{D}	$N(\pi)$	$N(\nu)$	\mathcal{R}
^{108}Sn					
7.56	7	0.048	0.132	0.868	0.014
8.67	13	0.078	0.874	0.126	0.007
9.89	11	0.066	0.058	0.942	0.000
16.53	21	0.126	0.476	0.524	0.546
^{114}Sn					
7.95	9	0.053	0.422	0.578	0.022
8.35	13	0.076	0.583	0.417	0.024
9.88	6	0.035	0.025	0.975	0.000
16.33	24	0.140	0.448	0.552	0.511
^{116}Sn					
7.98	7	0.040	0.498	0.502	0.021
8.38	14	0.081	0.530	0.470	0.028
9.88	3	0.017	0.011	0.989	0.000
16.27	24	0.139	0.509	0.491	0.569
^{128}Sn					
7.88	9	0.051	0.166	0.834	0.053
8.31	11	0.062	0.805	0.195	0.005
9.99	7	0.039	0.067	0.933	0.003
17.03	17	0.096	0.425	0.575	0.450
^{132}Sn					
7.88	7	0.038	0.038	0.962	0.018
8.13	12	0.066	0.489	0.501	0.022
10.02	14	0.077	0.130	0.870	0.007
16.92	17	0.093	0.483	0.517	0.513

Table VII: Same as in Table IV for the 1^- states of the various tin isotopes identified by the arrows in Fig. 9.

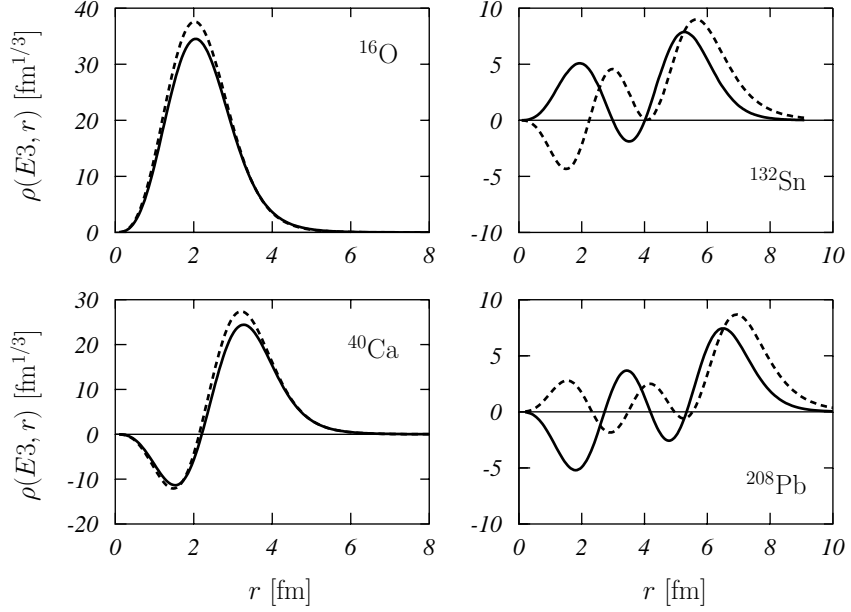


Figure 1: Transition densities for the 3^- low-lying states of the ^{16}O , ^{40}Ca , ^{132}Sn and ^{208}Pb nuclei. The full lines indicates the proton transition densities, and the dashed lines the neutron transition densities. Here, and in the following figures, we drop dependence on ω with respect to the definition (5), since each transition density is calculated for a specific value of the excitation energy.

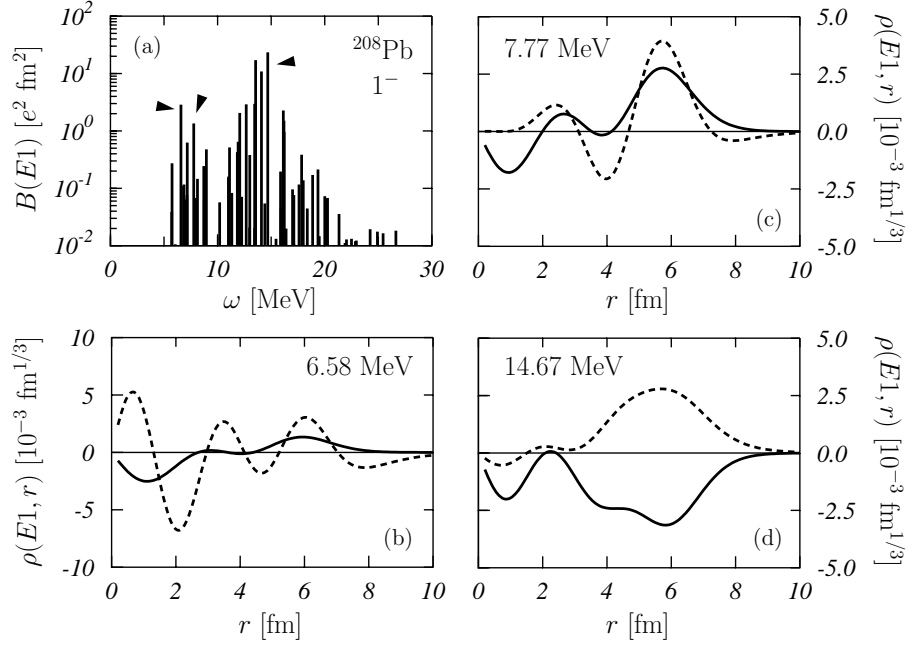


Figure 2: Dipole results for the ^{208}Pb nucleus. In panel (a) we show, in log scale, the $B(E1)$ values as a function of the excitation energy. In the other panels, we show the transition densities for the states indicated by the arrows, whose excitation energies are given in the panels. In panels (b), (c) and (d) the meaning of the lines is the same as in Fig. 1.

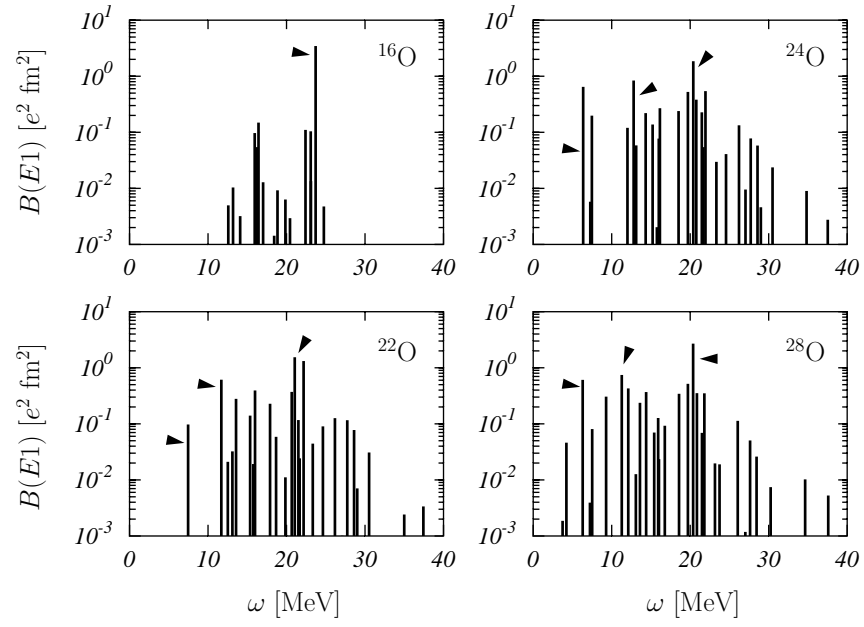


Figure 3: $B(E1)$ distributions for the oxygen isotopes we have studied. The numbers in the panels indicate the mass number of the isotope. The collectivity indexes of the states indicated by the arrows are given in Table IV.

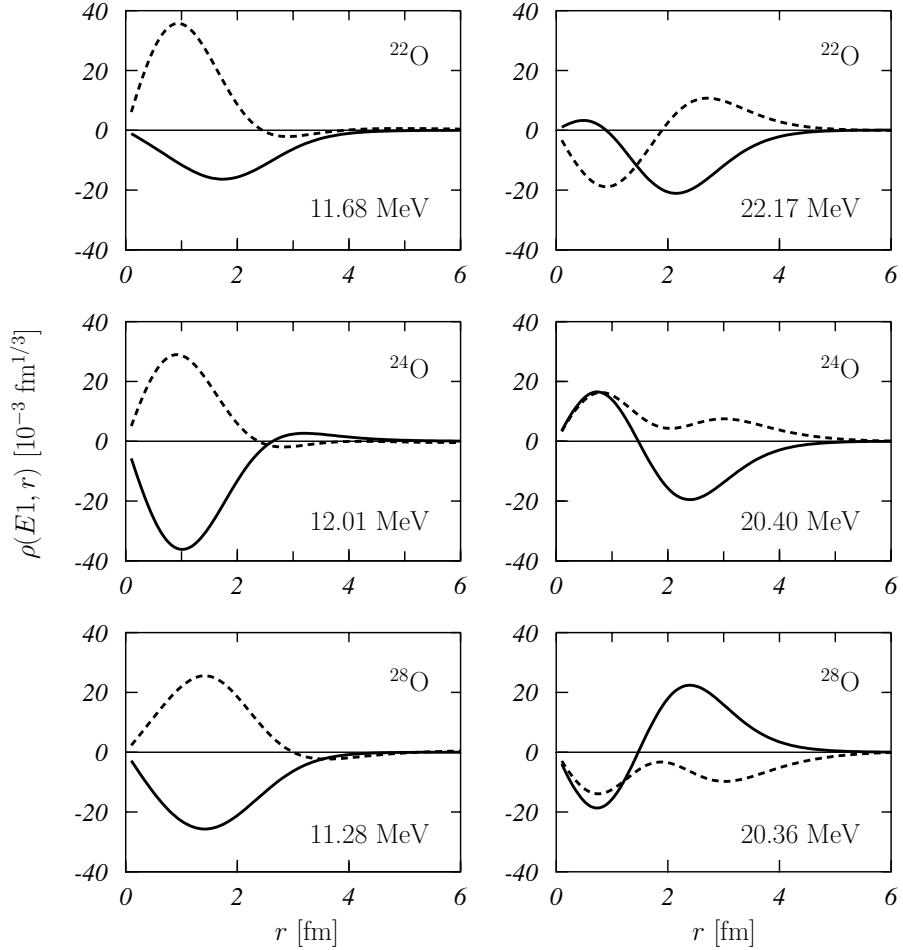


Figure 4: Transition densities, multiplied by a factor 1000, of some 1^- states for various oxygen isotopes. The numbers in the panels indicate the excitation energy in MeV. Full and dashes lines represent proton and neutron densities, respectively.

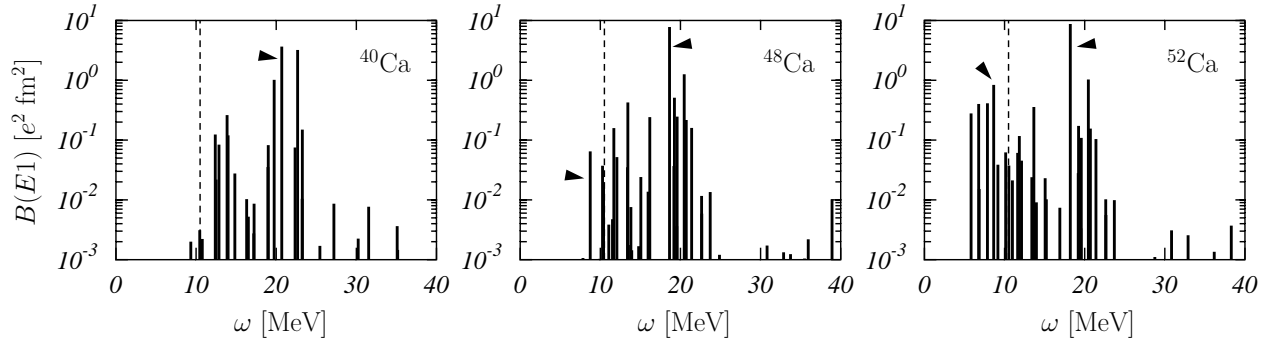


Figure 5: Same as in Fig. 3, but for the calcium isotopes we have studied. The collectivity indexes of the states indicated by arrows are given in Table V. The meaning of the dashed line is explained in Fig. 11 and in the related text.

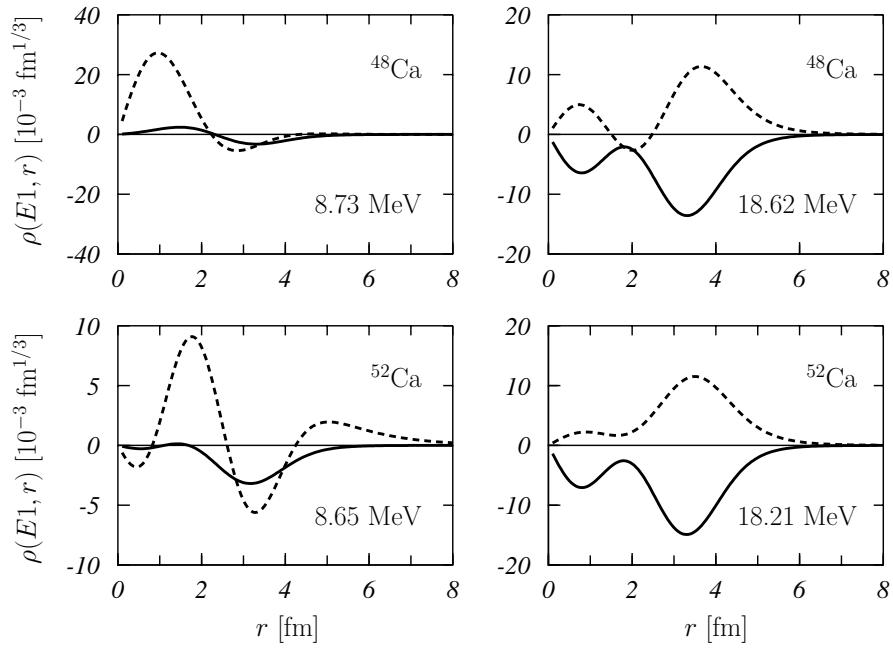


Figure 6: Same as in Fig.4, but for various calcium isotopes.

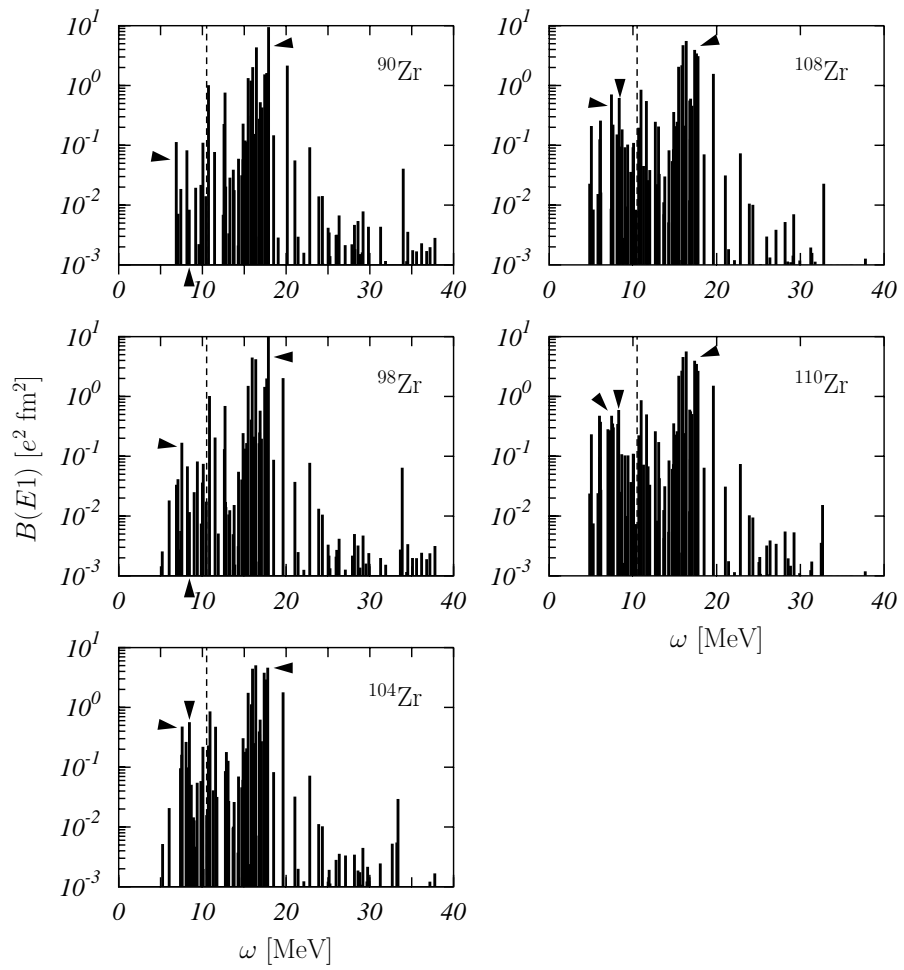


Figure 7: Same as in Fig. 3, but for the zirconium isotopes we have studied. The collectivity indexes of the states indicated by arrows are given in Table VI.

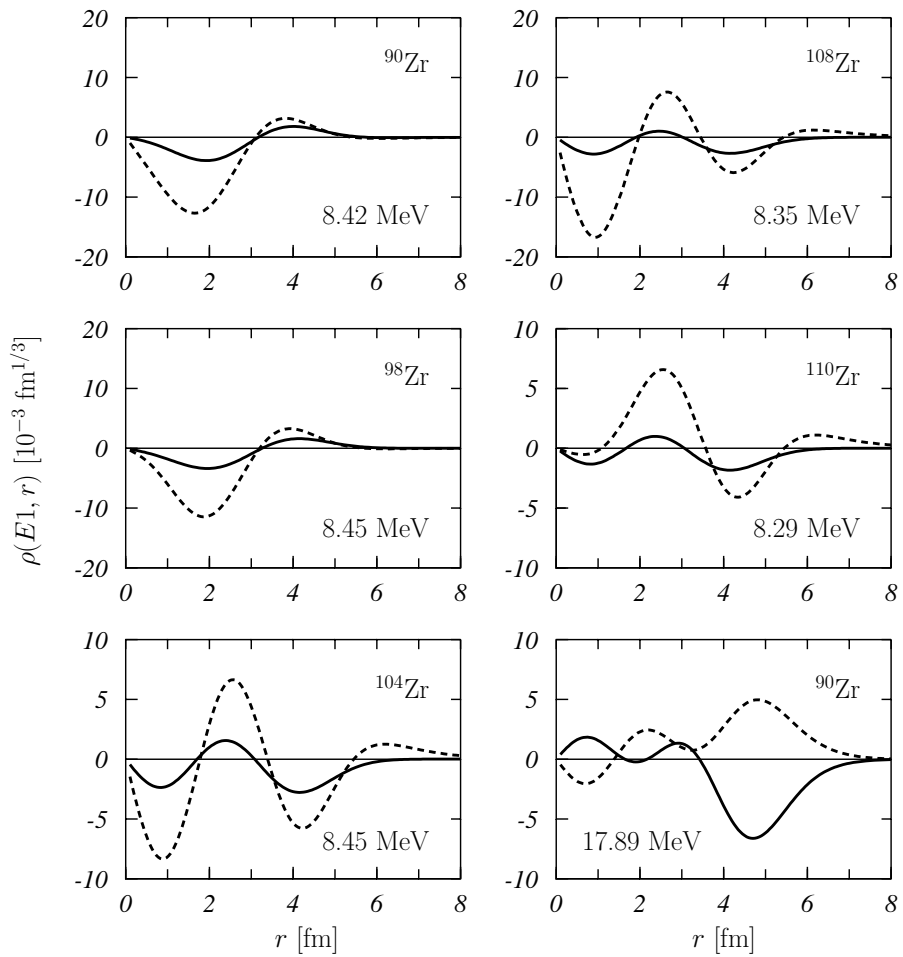


Figure 8: Same as in Fig. 4, but for various zirconium isotopes.

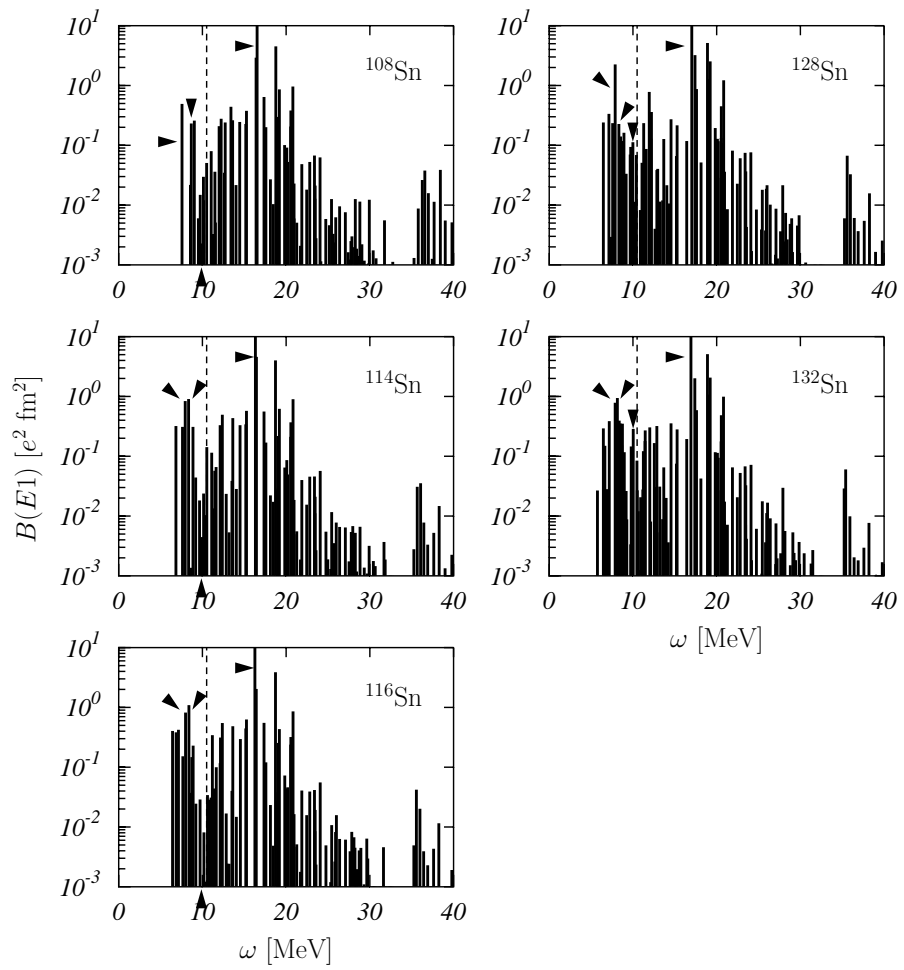


Figure 9: Same as in Fig. 3, but for the tin isotopes we have studied. The collectivity indexes of the states indicated by arrows are given in Table VII.

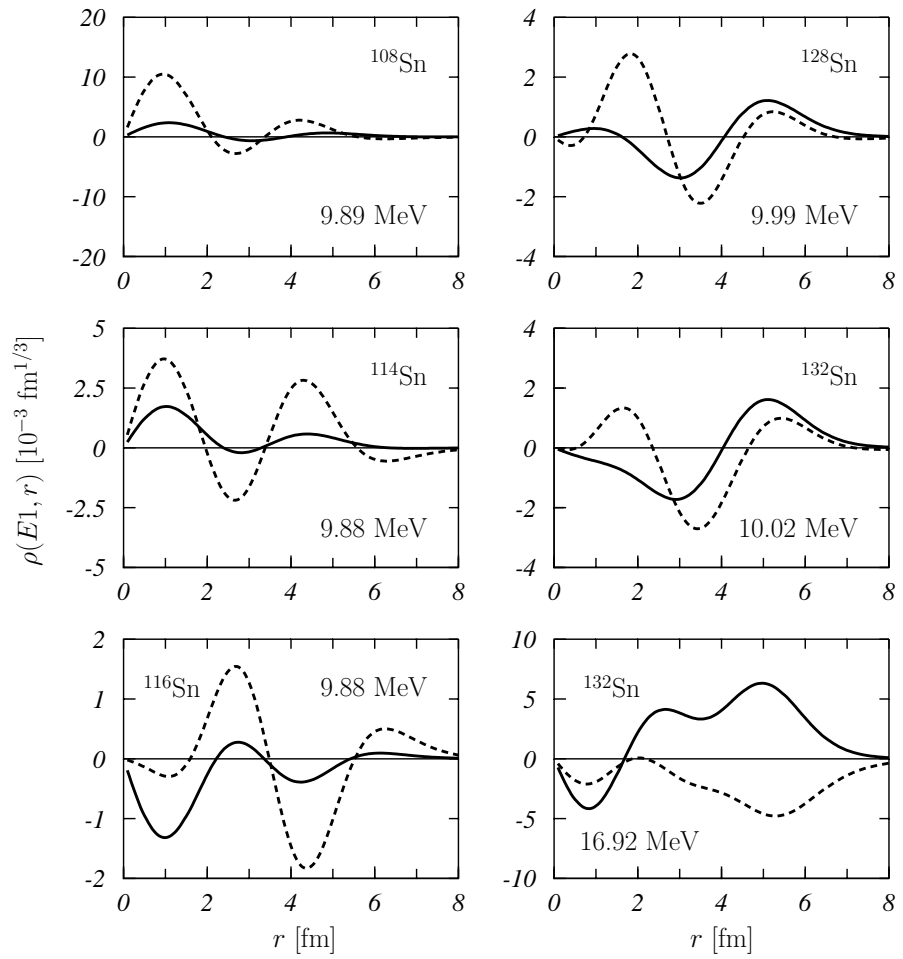


Figure 10: Same as in Fig. 4, but for the tin isotopes we have studied.

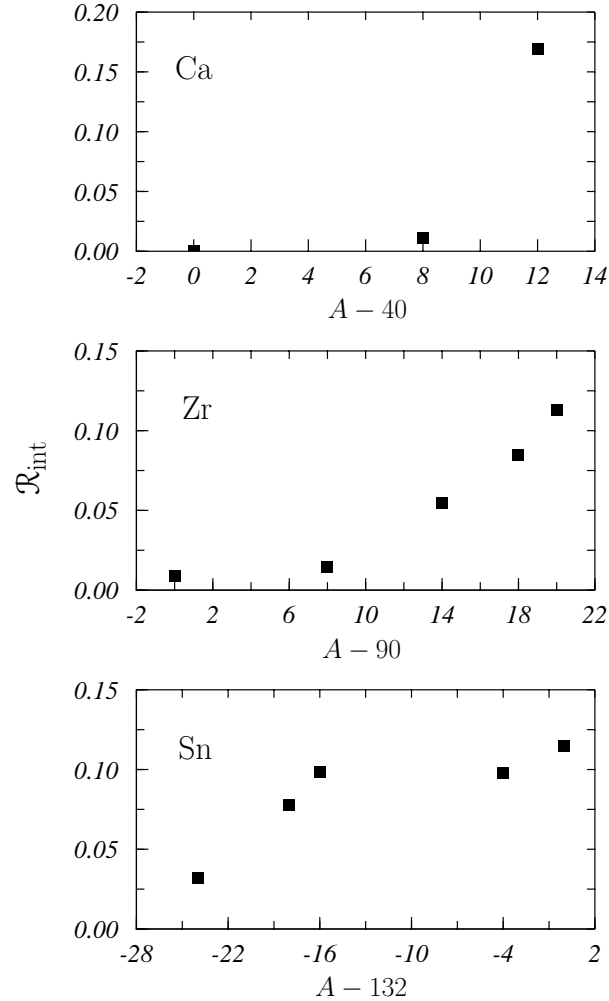


Figure 11: Ratios \mathcal{R}_{int} between the integrated $B(E1)$ values of the PDR, and the global $B(E1)$ strength against the number of neutrons in excess with respect to the doubly magic core of the Ca, Zr and Sn isotopic chains. The $B(E1)$ values of the PDRs have been obtained as a sum of all the values below the dashed lines indicated in Figs. 5, 7 and 9.

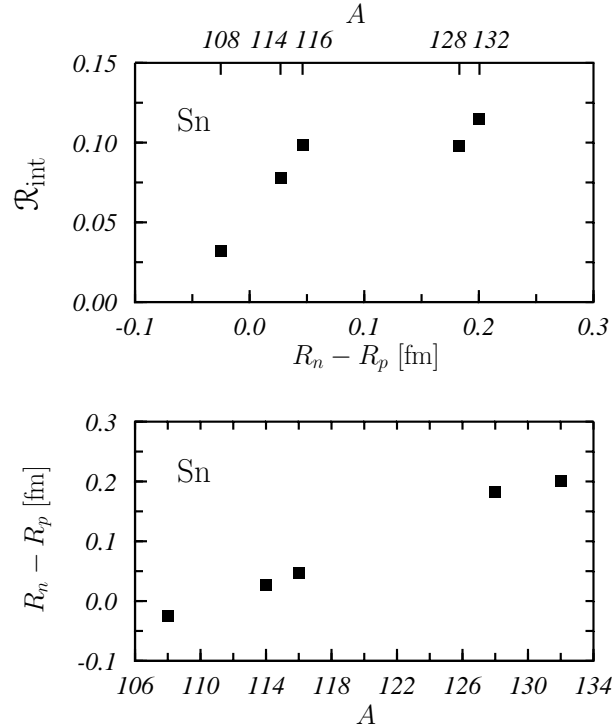


Figure 12: Top panel: ratio \mathcal{R}_{int} between the integrated $B(E1)$ values of the PDR, and the global $B(E1)$ strength against the difference between the proton (R_p) and neutron (R_n) root mean square radii for, from left to right, $A=108, 114, 116, 128$ and 132 Sn isotopes. Bottom panel: difference $R_n - R_p$ as a function of the mass number A .